DALHOUSIE UNIVERSITY

A High Resolution Record of Sediment Deposition in the Gulf of Aqaba during the last ~4000 years

Ariel Greenblat

SUBMITTED IN PARTIAL FULFILLMENT OF THE REQUIREMENTS FOR THE DEGREE OF
BACHELOR OF SCIENCES, HONOURS
DEPARTMENT OF EARTH SICENCES
DALHOUSIE UNIVERSITY, HALIFAX, NOVA SCOTIA

March 30, 2018

Distribution License

DalSpace requires agreement to this non-exclusive distribution license before your item can appear on DalSpace.

NON-EXCLUSIVE DISTRIBUTION LICENSE

You (the author(s) or copyright owner) grant to Dalhousie University the non-exclusive right to reproduce and distribute your submission worldwide in any medium.

You agree that Dalhousie University may, without changing the content, reformat the submission for the purpose of preservation.

You also agree that Dalhousie University may keep more than one copy of this submission for purposes of security, back-up and preservation.

You agree that the submission is your original work, and that you have the right to grant the rights contained in this license. You also agree that your submission does not, to the best of your knowledge, infringe upon anyone's copyright.

If the submission contains material for which you do not hold copyright, you agree that you have obtained the unrestricted permission of the copyright owner to grant Dalhousie University the rights required by this license, and that such third-party owned material is clearly identified and acknowledged within the text or content of the submission.

If the submission is based upon work that has been sponsored or supported by an agency or organization other than Dalhousie University, you assert that you have fulfilled any right of review or other obligations required by such contract or agreement.

Dalhousie University will clearly identify your name(s) as the author(s) or owner(s) of the submission, and will not make any alteration to the content of the files that you have submitted.

If you have questions regarding this license please contact the repository manager at dalspace@dal.ca.

Grant the distribution license by signing and dating below.

_____ _____

Name of signatory Date

Abstract

The Gulf of Aqaba is a narrow and deep basin at the northeastern tip of the Red Sea. Sedimentation is dominated by biogenic and aeolian material, as well as by material delivered by various wadis surrounding the Gulf. Here we present paleoenvironmental proxy records from a 107 cm gravity core, recovered at 720 m water depth at the northern end of the Gulf. Radiocarbon dating suggests that this core covers the last ~4000 years. Sediment flux directly sampled by co-located sediment traps deployed since 2014 shows that sedimentation is dominated by sporadic, short-lived flux events. These events transport large quantities of terrestrial material, manifested by the down core Fe/Al record, which displays an inverse relationship to the carbonate (%) record. Carbonate content, foraminiferal abundances, and bulk sediment elemental composition (determined by ICP-MS) will be discussed in the context of environmental and hydrographic variability. The carbonate content ranges between 25-45%, and generally co-varies with changes in planktonic foraminiferal abundances (0-50/g (wet sediment). The most prominent interval within the core is an instantaneous event deposit at 96-87 cm (~810 BC) containing allochthonous material in a fining upward sequence. This period is tentatively ascribed to a turbidite triggered by an earthquake. Several stratigraphic periods will be discussed in attempt to reconstruct recent geological and paleoceanographic patterns influencing the Gulf of Aqaba.

Keywords: sedimentation rates – age model – carbonate – foraminifera – elemental ratios – turbidite

Table of Contents

List of Figures

List of Tables

List of Abbreviations

LSR- linear sedimentation rate
GoA- Gulf of Aqaba
PF- planktonic foraminifera
g_{ws}- gram of wet sediment
PSU- Practical Salinity Unit

Acknowledgements

Beyond the graphs and tables, this honours thesis is a testimony to my dedication to learning and interest in uncovering the mysteries of the world around us. Having the opportunity to do research in Israel, a place that is special to me and my family, was a fulfilling experience that I am incredibly grateful for.

I would like to thank Dr. Markus Kienast, my Dalhousie supervisor, who has exceeded his regular responsibilities as a mentor and has given me space to be self motivated while also providing his unwavering guidance. I am grateful for the discussions we had and the patience he bore through my confusion and struggles.
Thank you to Dr. Stephanie Kienast and Mr. Lachlan Riehl for the Sediment Trap Data, as well as the members of Kienast lab group for your support and advice along the way.

I would like to the thank Dr. Adi Torfstein, my supervisor in Israel, at the IUI, for making my stay in Israel a positive experience. Adi provided me with many unique learning opportunities in the lab and taught me to think critically and work efficiently in a lab setting.

I owe a big thank you to Natalie Chernihovsky for her expertise, patience and all her help in Foraminifera identification. Her persistence and wealth of knowledge about tiny little creatures that live in the sea is impressive and inspiring. Her contributions are evident in many parts of this thesis. I am grateful for the maternal role she took on while I was at the IUI.

I would also like to thank Mr. Barak Yarden, the lab technician at the IUI for his patience, responsible character and for always willing to help. Finally, I would like to thank Moti and Akos at the IUI for their help with the calcimeter apparatus.

Most of all I would like to thank my family in Israel and Toronto for the unconditional support and love they have given.

Chapter 1: Introduction

1.1 Overview

Chemical and biological indicators in the sediment record, termed proxies, are often used by scientists to reconstruct past environmental and oceanographic settings, on the scale of tens of thousands to millions of years. Sediment records can help us to understand major climate events and are commonly used to predict future climate fluctuations observed within the proxy record. Sediments are composed of biogenic and terrigenous material. The biogenic components are silica or carbonate based. Siliceous organisms include diatoms and radiolaria, while the carbonaceous organisms include foraminifera, pteropoda, cocolithophora and reef fragments. These biogenic sediments can be used to provide a record of past surface water temperatures, ocean circulation patterns and nutrient availability. Terrigenous material is deposited via aeolian or fluvial mechanisms which provide information about sediment provenance. The purpose of this study is to reconstruct the paleoenvironmental conditions based on sedimentation rates, foraminiferal abundances and sediment composition using carbonate (%) and geochemistry ratios to acquire a better understanding of the processes that dominate the Gulf of Aqaba, located in northern Red Sea. This honours project will investigate a ~4000 year record at a 1-cm resolution on a sediment gravity core recovered from 720 m water depth.

In this study, the term Gulf is referenced to the Gulf of Aqaba.

The Red Sea is a unique area of study for paleoclimatologists due to its warm and saline waters and limited replenishment of sea water from the Indian Ocean. Lack of sea water exchange affects the nutrient input and salinity levels and therefore has significant implications on the biogenic components of the sediment. Because the Red Sea is located in an arid region, the low vegetation cover and surrounding mountains make this region susceptible to flash flooding, resulting in rapid sediment deposition. Mineral dust from the Saharan desert also accounts for a significant proportion of the annual sedimentary input in the Red Sea (Palchan et al., 2013) .

1.2 Geological setting

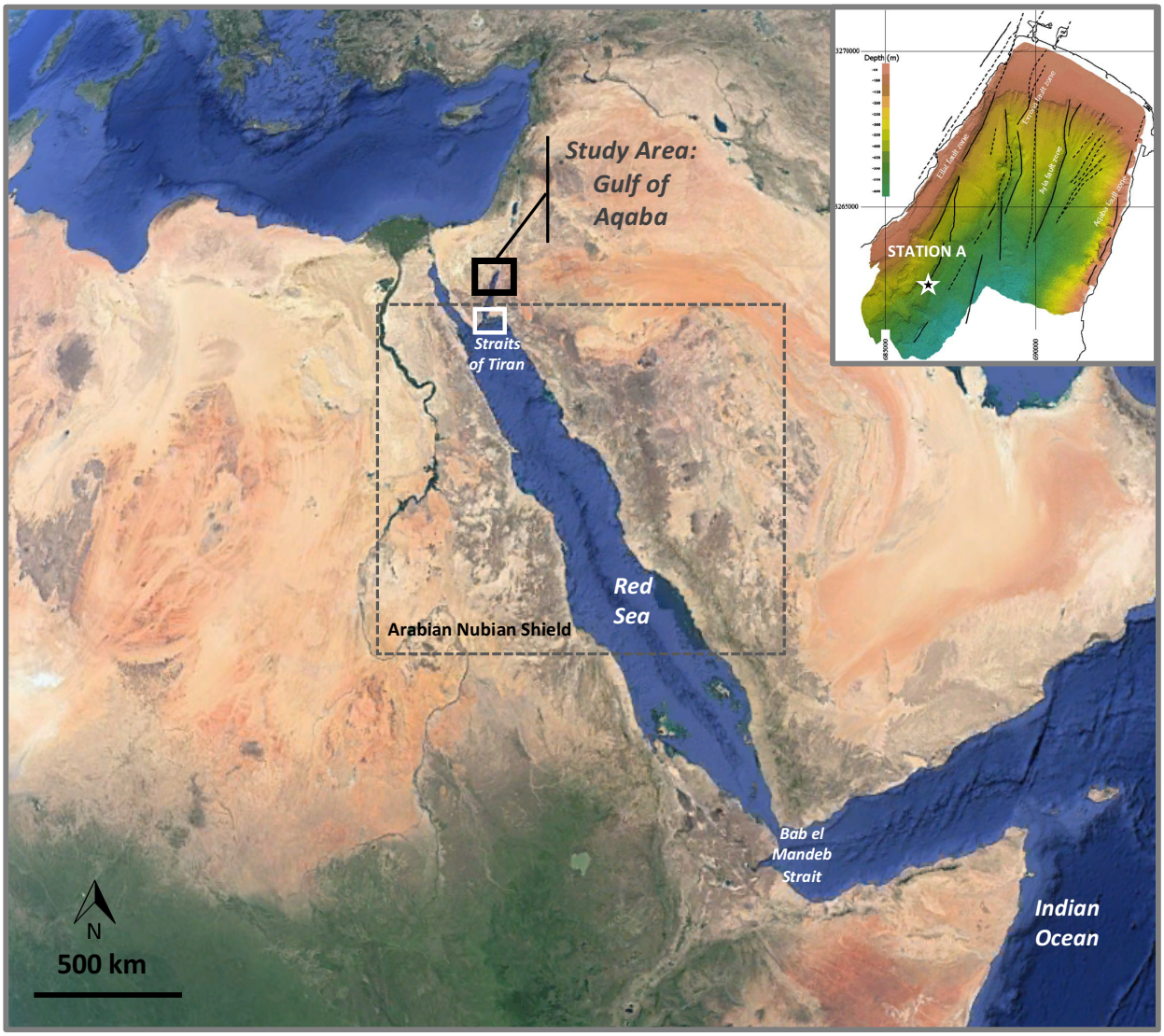

Figure 1 LANDSAT image of study area and important locations (GoogleEarth 2018). Inset map showing bathymetry obtained by MBES and location of sampling site (Station A) (Tibor et al. 2010) .

The Gulf of Aqaba is an elongated (180 km), narrow, (10-26 km wide) and deep (1830 m at maximum depth) basin located at the northern tip of the Red Sea (Fig 1.) (Friedman, 1968; Steiner et al., 2016 and Reiss & Hottinger, 1984). Infrequent precipitation (22 mm y^{-1}) which typically occur between December and February (Reiss and Hottinger et al., 1984 and Friedman, 1968) bring large masses of terrestrial material from the surrounding crystalline basement through various surrounding Wadis such as Wadi Mubarak, Wadi Arava and Wadi Yutim (Lamy

et al., 2006 and Shaked et al., 2002). Records of floods are characterized by clay sized sediments, while terrestrial material is typically comprised of fine to medium size grained sand (Katz et al., 2015). Current research on the Gulf investigates whether sediments transported via flooding events reach the deeper part of the basin, or if they are restricted to shallow waters (Pers. Comm. Kalman). There are instances, however, where sediments are known to reach great depths and travel long distances due to the presence of the Arava fan (Tibor et al., 2010). The Gulf formed during the Cenozoic due to the separation of the Arabian Nubian Shield (ANS), a large craton composed of primarily silicic magmatic and metamorphic mountains (Fig. 1) (Goodman et al., 2016). Eroded sediments from these mountains get deposited in the Gulf via flash floods, producing hyperpycnal flows (sediment saturated waters that are denser than the Gulf's water) (Katz et al., 2015).

Furthermore, fine sediment particles transported by winds from the Saharan desert are constantly deposited in the Gulf (Palchan et al., 2013) with super imposed dust storms which show a mass accumulation rate of 35 g/m^2/year (Katz et al., 2015, Goodman et al., 2016; Steiner et al., 2016 and 2017, Al-Taani et al., 2014).

1.3 Susceptibility to mass movement

The Gulf of Aqaba is susceptible to earthquakes and tsunamis due to its location at the terminus of the Dead Sea Transform (DST) Fault (Migowski et al., 2004). Geological evidence and historical archives document earthquakes in the Aqaba region during the late Holocene with a recurrence interval of 1.2 ± 0.3 ka with an average slip rate of 2.3-3.5 mm/year (Kanari et al., 2015; Goodman-Tchernov et al., 2016 and Migowski et al., 2004). Increased documentation of earthquakes is also a result of human population increase over the past 2800 years as this region was a major migratory route. The submarine Avrona fault, an active segment of the DST fault, between the Sinai sub-plate and the Arabian plate, accommodates most of the sinistral strike-slip movement (Kanari et al., 2015). Bouma sequences and large abundances of coral reef fragments are attributed to mass movement events (Almogi-Labin et al., 1996). Mass movement events are manifested in the sedimentary record by laterally continuous allochthonous deposits as well as higher abundances of eroded, blackened, yellowed and larger than average foraminifera (Goodman-Tchernov et al., 2016).

A study by Migowski et al. (2004) correlated known ages to anomalous sequences found in multiple submarine cores from the region. They concluded that coarse grains were deposited via earthquake events rather than flash flooding or spontaneous slump deposits. However, an anomalous bed in the Tchernov-Goodman et al. (2016) sediment core also featured higher concentrations of larger mixed shell and coral fragments suggesting high energy transport events such as tsunamis (Goodman- Tchernov et al., 2016).

1.4 Oceanographic setting

The Gulf of Aqaba experiences high evaporation rates (200 cm y^{-1}) which produces high surface salinities (40.6 ‰) and warm (21.7°C) surface temperatures. Mixing between surface and subsurface layers plays a major role in determining the physical and biogeochemical properties of marine environments (Wurgaft et al., 2013). Circulation of surface waters in the northern Gulf is primarily driven by south-easterly winds bringing in nutrient depleted water from the Red Sea over the Bab-el-Mandeb strait (Fig. 2) (Reiss and Hottinger, 1984, Arz et al., 2003; Lamy et al., 2006 and Edelman-Furstenberg et al., 2001). During the late Holocene, the Gulf fluctuated between humid and arid climates causing changes in water stratification due to the intensification of the Mediterranean and monsoonal climate systems which are driven by changes in the inter tropical convergence zone (Edelman-Furstenberg et al., 2009; Kumar et al., 2018). Foraminifera are excellent proxies to infer changes in circulation and climate because they are sensitive to changes in salinity, sea water temperatures and nutrient availability (Reiss and Hottinger, 1984).

N

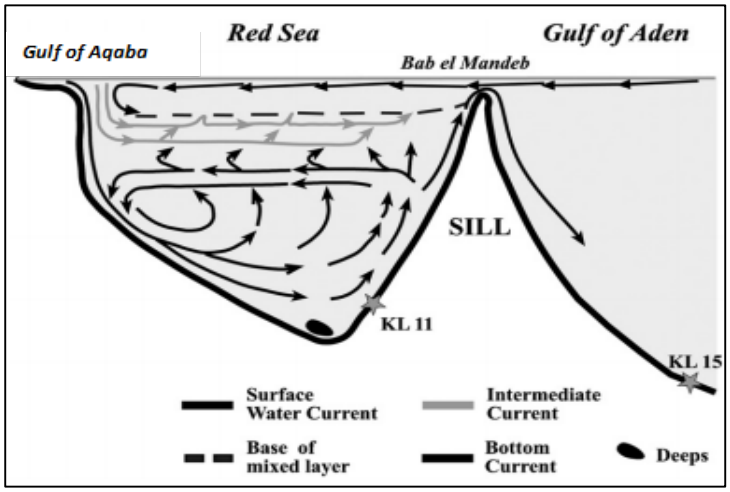

S

Figure 2 Schematic transect of Red Sea showing main water current over the Bab el Mandeb Strait (Stein et al., 2007).

Chapter 2: Methods

The GoA core was recovered from 720 m water depth from Station A (Fig. 1) on October 16, 2016, using a gravity core. A gravity core consists of a metal pipe with a removable plastic lining with a heavy weight that sits on top. The core is lowered over the side of the Research Vessel using a winch and wire and is allowed to free fall into the sediments.

The following analyses were performed on a cm level resolution.

2.1 Carbonate (%)

Carbonate (%) was measured using a "carbonate bomb" (also known as a calcimeter) on aliquots of dried sediment (Fig. 3). Sediment was homogenized with a mortar and pestle and weighed at 1.00 ± 0.10 g and then placed in an airtight chamber. 20 mL of 10% HCl was injected into the chamber through the luer valve using a plastic syringe. Constant pressure was applied using a polyethylene syringe holder for the duration of the experiment to limit CO_2 dissipation. The apparatus was then placed on a magnetic stirring plate to ensure all sediments were exposed to hydrochloric acid (HCl). Acid was added in excess to ensure all sediments were reacted. After 30 seconds, pressure was recorded. CO_2 build up is proportional to the amount of calcite or dolomite found in the sample (Eq.1).

Figure 3 Calcimeter-Pressure Gauge Model (Fann Insturment

$$CaCO_3(s) + 2HCl\ (l) \rightarrow CaCl_2\ (s) + CO_2\ (g) + H_2O\ (l)\ (Eq.1)$$

After 20 minutes a second reading was recorded. This measurement is associated with full dissolution of the dolomite component of the sediments since there was limited to no change in pressure (Fig. 4) (OFITE instruction manual and personal observations).

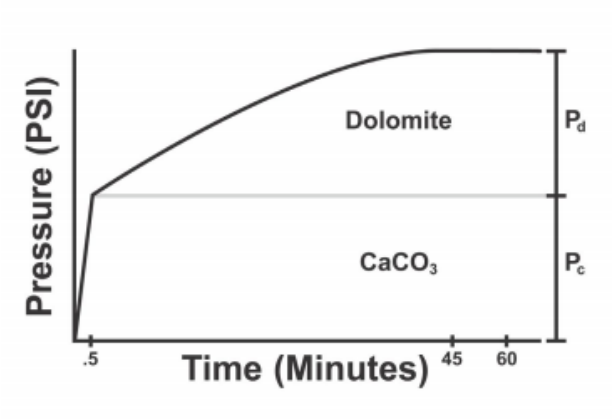

Figure 4 Interpretation of pressure reading. Measurements were obtained in PSI units and then converted to kPa. (OFITE instruction manual, 2015)

A third reading at 30 minutes was recorded to determine whether there was a change in pressure. Approximately 10% of samples showed an increase in pressure which exceeded the standard deviation (ΔP=2.36 kPa) at the 30 minute reading. However, samples that were obvious outliers, likely related to CO_2 dissipation or aggregated sediments, were reanalyzed to decrease uncertainties. The stainless-steel spatula, magnet, syringe and carbonate bomb chamber were cleaned with Kim wipes, moistened by 95% ethanol, and rinsed with Milli-Q® water between each analysis.

2.1.1 Calibration Curve

Pure calcium carbonate ($CaCO_{3\ (s)}$) powder was the carbonate standard. By using a known weight of pure CaCO3, the relationship between the amount of CO_2 released and the amount of carbonate in the sample can be determined using a calibration curve. The analytical procedure for creating the calibration curve is identical to the above protocol for sediments. Four calibrations were done (Fig. 5) on varying masses of pure $CaCO_3$, ranging from 0.1 to 0.7 g. All calibrations were plotted together to obtain a slope = 189.4 and an r^2 = 0.996 (Fig. 6). Using this slope, pressure readings were converted to carbonate % (Eq. 2 and 3). Calibrations were executed approximately every 20 samples.

$$CaCO_3(\%) = \frac{P_i - P_s}{Sample\ Weight * Slope}\ (100)$$ *(Eq.2, used for reading after 30 seconds)*

P_s – syringe pressure

P_i – initial reading of pressure gauge (calcite)

$$Ca, Mg(CO_3)_2\ (\%) = \frac{P_f - P_s}{Sample\ Weight * Slope}\ (100) \qquad (Eq.3\ ,\ used\ for\ reading\ after\ 20\ minutes)$$

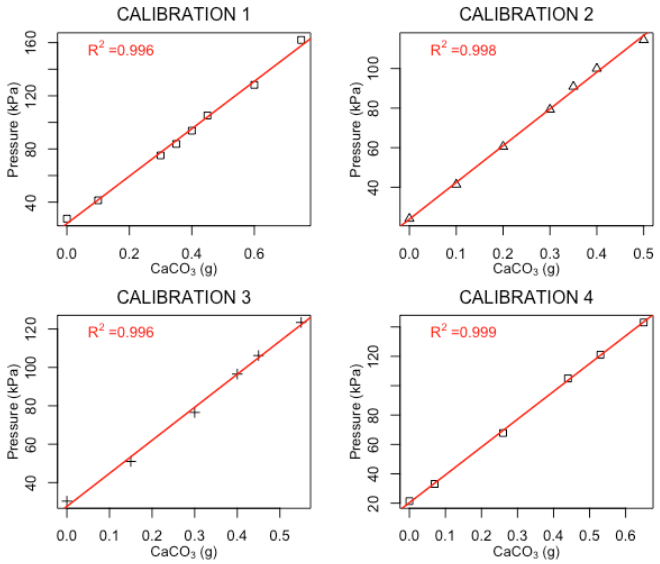

Figure 5 Calibration curves performed every 20 sediment samples for varying masses of pure $CaCO_3$. Used to determine relationship between pCO_2 and $CaCO_3$

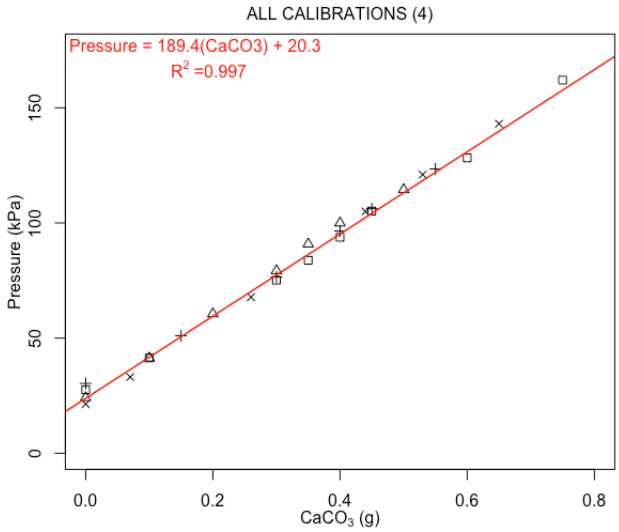

Figure 6 Combined calibrations with slope used to correlate pressure to carbonate (%)

2.1.2 Propagation of error

The standard deviation was calculated on replicates tested during the calibration stage. Pressure readings that correlate to $CaCO_3$ samples that were measured more than once, example, 0.00 g, 0.30 and 0.45 g were used to measure the standard deviation and used in Eq. 2, as variable "P_i" to determine the percent error (1σ (68%) = 1.5%) (Fig. 6). During the weighing process the sediments were exposed to air which may have shown a higher mass reading due to added moisture weight. Scale readings were only accurate to 2 decimal places. Changes to force injection pressure were also variable and would therefore affect the initial reading at 30 seconds ("P_i").

2.2 Foraminifera picking and identification

Approximately 4 g of wet sediment aliquots were wet sieved with Milli-Q® water through a 125 µm stainless steel mesh sieve. Collected sediment (125-300 µm (approximated upper bound) was oven-dried at 60 °C until fully dried. Foraminifera were identified, hand-picked and

counted for planktonic foraminifera under a Leica® stereoscopic microscope. *Globigerinoides ruber* and *Globigerinoides sacculifer* were separated, while the remaining species were grouped together as an "other" category. Species were generally well preserved with minimal erosion or discolouration. Broken individuals were excluded from counts to avoid misidentification. Identification and picking were done at the Interuniversity Institute for Marine Sciences in Eilat and at Dalhousie University.

2.3 Geochemistry analysis

The following analyses were carried out at the Joint Interuniversity Institute (IUI), in Eilat, by Barak Yarden, in the clean lab facilities. The protocol described below is adopted from Steiner et al., 2017. The major and trace element compositions were analyzed for it's bulk, silicate and carbonate fractions (Table 1). The core was sectioned every 1 cm and dried for one week at 60 °C. Subsequently, the samples were rinsed three times in Milli-Q® water to remove interstitial salts, dried again and homogenized using an agate mortar and pestle. Approximately 100 mg were weighed and digested as a bulk fraction using a mixture of concentrated HNO_3-HF on a hotplate. Typically, full dissolution was achieved within ~2 digestion cycles, after which the sample was dried and residual fluorides were removed by re-dissolution in concentrated HNO_3, heat fluxing and drying at ~150 °C. This step was repeated twice. The dried residue was then dissolved in 5 mL of 4 N HNO_3 and aliquots were extracted and diluted ~2000-fold using a 3% HNO_3 solution. These were measured for their elemental abundances by an ICPMS Agilent 7500cx. Analyses were calibrated with several sets of multi-element gravimetric standard solutions together with the addition of internal spikes of known concentrations (50 µg/L Sc and 5 µg/L Re and Rh). All lab work was performed in the clean lab of the Interuniversity Institute for Marine Sciences, under a class 1000 environment, using pre-cleaned Teflon beakers and tips, and double distilled HNO_3 and HF acid solutions. In addition, splits of the dry powder were leached in 0.5 N HNO_3 until bubbling ceased. The dissolved fraction was dried and processed for chemical analyses as described above. This fraction represents the chemistry of the carbonate fraction. Another set of splits of the dry bulk powder were further leached in 3 N HNO_3 followed by 5% H_2O_2 to remove carbonates and oxidize organic matter. The residue, considered

to represent the silicate mineral phase, was then fully digested and processed for chemical analyses as above.

Table 1 Operationally defined phases for geochemistry analysis

Phase	Operationally defined reacted component
L	Carbonate
X	Organics
R	Silicate/ Residues

2.4 Radiocarbon dating

Planktonic Foraminifera (PF): *Globigerinoides ruber* and *Globigerinoides sacculifer,* with no evidence of impurities or eroded chambers, were handpicked for radiocarbon (^{14}C) dating. Approximately 6 mg of Foraminifera (~200 shells/sample) were collected from 6 intervals varying between 1- 4 cm in thickness (Table 2). For some intervals, foraminiferal mass in individual cm layer were below the required amount and therefore intervals from above or below were added. No intervals were chosen above 45 cm because ages determined from a co-located core are superimposed on the age model attributed to the GoA core. This will be further discussed in section 3.3.1. Two intervals bounding 82 cm, 83 cm and 100 cm, 101 cm and including 96 cm, an anomalous sediment sequence, were also chosen for radiocarbon dating. This will also be further discussed in section 3.2. The calibration of radiocarbon ages from marine samples requires age correction due to isotopic fractionation. Radiocarbon dating in the Red Sea varies due to different rates of water exchange through the Bab el Mandab straits (Trommer et al., 2010). A Marine Reservoir correction (ΔR) of 170 years, proposed by the Marine Reservoir Correction Database compiled by P. Reimer, will be used for this age model. Studies in the Red Sea use a ΔR value between 100-180 years (http://www.depts.washington.edu/qil/marine/). A 400 year offset is also incorporated to the calibration to account for the average global reservoir effect (Stuiver et al., 1998). Specimens were ultrasonicated and rinsed repeatedly with Milli-Q ® ultrapure water (18.2 MΩ) to remove terrigenous inputs. Radiocarbon dating was undertaken by an Accelerator Mass Spectrometer (AMS) at the Poznań Radiocarbon Laboratory Poland. Radiocarbon dates were calibrated using the CALIB radiocarbon software version 7.1 (Stuiver, M., Reimer, P.J., and Reimer, R.W., 2018,

CALIB 7.1). The “MARINE13” calibration data set was used as it pertains to tropical and subtropical records and is suitable for mid-latitudes in the northern hemisphere. This calibration curve is based on the ocean-atmosphere box diffusion model outlines by Oeschger et al. (1975). The calibrated ages are reported to 1 standard deviation in Table 2.

Chapter 3: Age model

Radiocarbon dating is used in paleoclimatology to establish the age of events that relate to sediment depth. Obtaining reliable ages is a fundamental process to infer past climate based on changes in past climate.

3.1 Sedimentation rates

3.1.1 GoA Core

This section will explore sedimentation rates from the GoA core, co-located records and a sediment core from the northern Gulf. The linear sedimentation rates (LSR) were determined by calculating the slope between each consecutive ^{14}C data point (Eq. 4). Sedimentation rates in the GoA core ranged from 0.01 cm/year to 0.07 cm/year over the last 4000 years as radiocarbon dating suggests (Fig. 7).

$$LSR = \frac{CoreDepth\ 2 - CoreDepth\ 1}{Age2 - Age1} \quad \textit{(Eq. 4)}$$

Table 2 Calibrated ^{14}C dates measured on G. ruber and G. sacculifer foraminifera.

Interval (cm in core)	***Age 14C BP*** *Uncalibrated*	***Error***	***Calibrated Years (Median Probability)***	***Lower Bound (1σ)***	***Upper Bound (1σ)***
45	1550	30	1023	991	1054
61,62,63	2080	30	493	446	538
82,83	2680	35	-235	-302	-177
96	4620	35	-2683	-2749	-2602
100,101	3625	35	-1385	-1434	-1342
104	3940	35	-1759	-1814	-1690

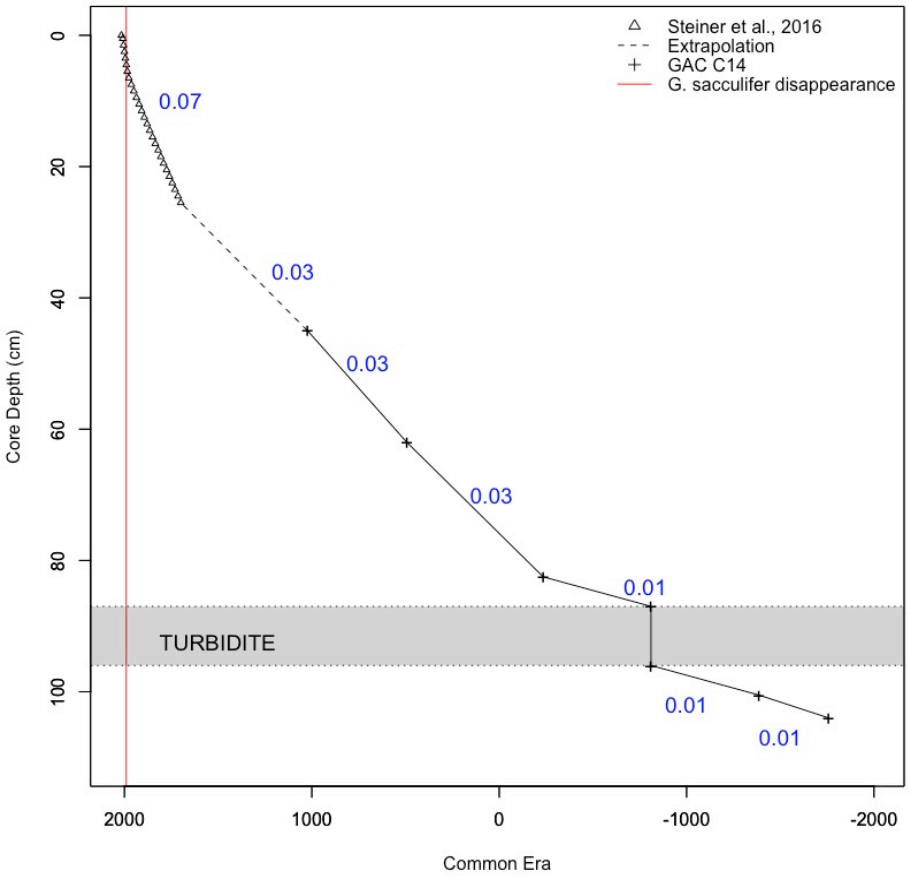

Figure 7 Age Model including linear sedimentation rates between each

3.1.2 Co-located sediment core

Sedimentation rates from a co-located sediment core are adopted for the top 45 cm of the GoA core. A LSR can be obtained for the top 45 cm of the GoA core by extrapolating from the first radiocarbon date (at 45 cm) to the top of the core (assumed to be the year when the core was recovered, 2016). This method resulted in a LSR of 0.045 cm/year. However, Steiner et al. (2016) used ^{210}Pb and ^{137}Cs activity to date 25 cm of sediments and extrapolated downwards to 35 cm from a core that was also recovered from Station A. The dating technique applied in their study is only suitable for dating sediments from the last 5 centuries (Steiner et al., 2016). Steiner et al.'s (2016) sedimentation rates should coincide with the GoA core extrapolated sedimentation rate since they are from the same locations and were recovered less than 2 years apart. Steiner et al. (2016) LSR can be separated into 2 distinct rates. The top 5 cm of the core features a LSR of 0.21 cm/year, while LSRs between 6 cm and 35 cm is 0.07 cm/year. They attribute the decrease in sedimentation rate to an exponentially decreasing bioturbation rate. A dotted line is featured between 25 and 45 cm to represent an interpolated LSR. No direct ages were obtained within this window and therefore uses known ages as anchor points (Fig. 7).

3.1.3 North Beach core

A sediment core recovered from the northern part of the Gulf (Lamy et al., 2006) resulted in sedimentation rates that were within the same order of magnitude as Steiner et al. (2016) and the GoA core (Fig. 9). The North beach core was recovered from an elevated ridge and was likely not exposed to turbidity currents (Lamy et al., 2006 and Ehrhardt et al., 2015). This core contains siliciclastic sands and carbonate sediments derived from living organisms, much like the sediments in the GoA core. Sediments are delivered by the Wadi Mubarak (labeled as a cone in Fig. 8) which are then delivered to the deep part of the basin, close to Station A. Interpretation of sedimentation rates and climatic variability will be further discussed in chapter 5 in the context of this core.

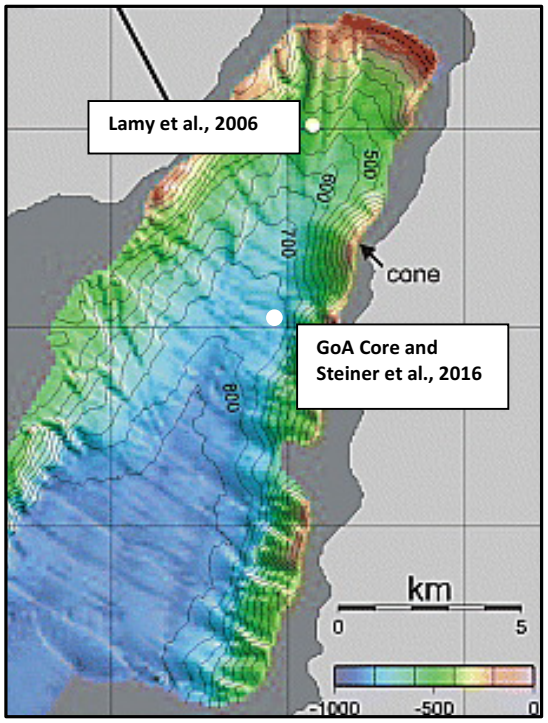

Figure 8 Lamy et al. (2006) core site

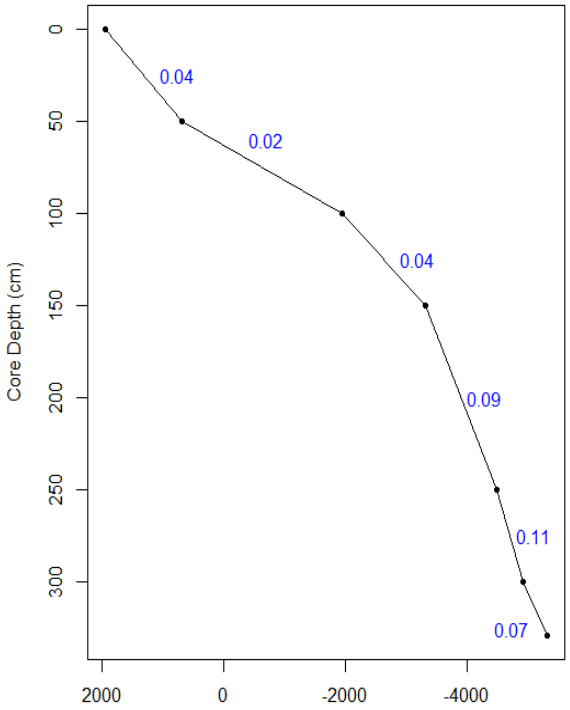

Figure 9 Linear Sedimentation Rates (Lamy et al., 2006)

3.1.4 Co-located sediment trap

Sediment traps are containers that are placed in the water to collect particles, such as organic matter, shells and dust. Sediment traps, located at Station A at 400 m water depth, were deployed since January 2014 (Fig. 10). Bulk flux was measured daily. These high resolution traps suggest that during the winter months, December to April, periods, on the order of days, have higher sediment flux compared to the remaining part of the year (May to November) (Fig. 11). A two-year average of bulk sediment flux is found to be 1.2 g/m^2 per day. Dividing by the sediment density (0.5 g/cm^3) yields a LSR of 0.09 cm/year. Due to the different temporal resolutions, it is likely that the GoA core, will deviate from the trap record. In addition, the sediment trap data alludes to events such as flash floods, that are muted by proxies with lower temporal resolution, such as the GoA core, Steiner et al. (2016) and Lamy et al. (2006).

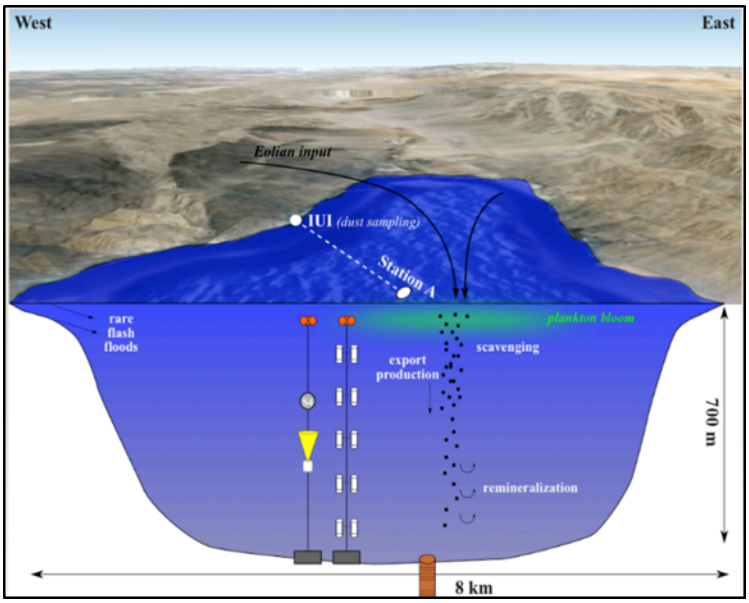

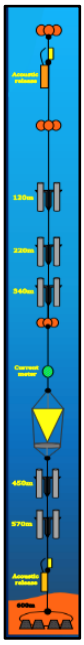

Figure 10 cross section view of McLane and KC Denmark traps (Torfstein, 2017)

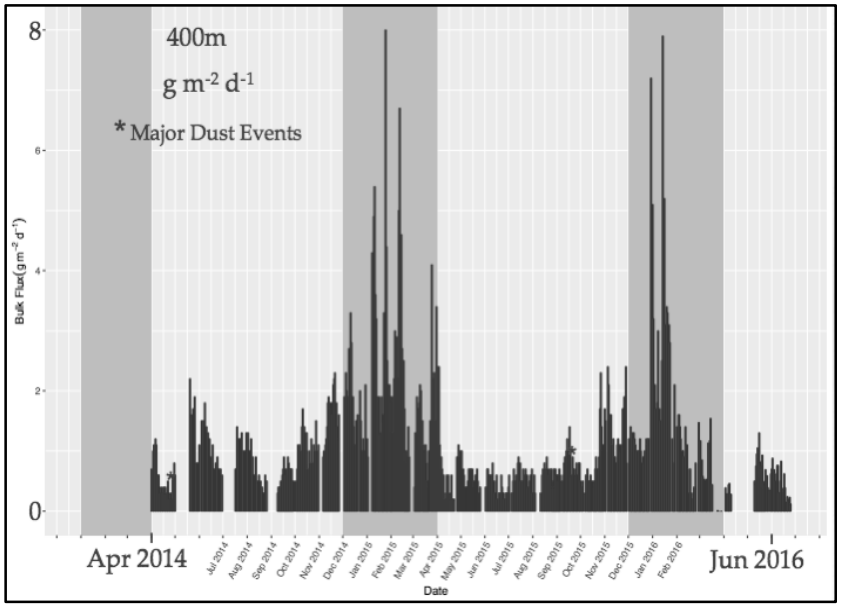

Figure 11 Annual time scale of bulk sediment flux (Riehl et al., 2017)

3.1.5 Core comparisons and summary

The GoA core, Steiner et al. (2006), Lamy et al. (2006) and co-located sediment trap data show LSRs within the same order of magnitude. Reasons as to why sedimentation rates differ are not known, however, because the cores and trap cover different lengths of time this may affect overall sedimentation rates due to compaction (Table 3). Overall, a common trend throughout the sediment core records is an increase in LSRs in the recent ~ 1000 years. Trap data also show highest LSRs and cover the most recent time period.

Table 3 Comparing Sedimentation rates for northern Gulf of Aqaba

Source	Average Sedimentation Rate (cm/year)
GoA Core	0.02
Steiner et al., 2016	0.07
Lamy et al. 2006	0.06
Sediment Trap	0.09

3.2 Turbidite deposit

The foraminifera shells that were dated at the 96 cm interval in the GoA core were older than those stratigraphically below. An anomalous sequence is observed between 87 cm and 96 cm and is attributed to a turbidite deposit triggered by an earthquake. The average age of the foraminifera from this interval is approximately 2683 BCE. Based on the bounding radiocarbon dates measured at 82 and 83 cm as well as 100 and 101 cm, this event likely occurred at approximately 810 BC. This age assignment was found using the midpoint of the two radiocarbon dates bounding the anomalous interval (235 BC and 1385 BC yields a midpoint of 810 BC). This is a reasonable method because the midpoint between the two bounding intervals is also the middle of the turbidite sequence with respect to the core depth.
This 9 cm interval is assumed to be instantaneous and is therefore depicted on the age model as a vertical line (Fig. 12).

A turbidite is sediment deposited by a turbidity current characterized by a fining upward sequence, similar to the sequence in the GoA core (Fig. 12). The bottom layers of this interval (96 ~ 94 cm) feature coarse reef fragments and an abundance of calcareous organisms such as

pteropoda and foraminifera (Fig. 13). Shaked et al. (2004), found a similar anomalously carbonate rich layer, abundant in Porite corals, assumed to have been a coral reef destroyed by an earthquake. Gradually, sediment becomes finer and more angular and presents higher concentrations of biotite, potassium feldspar and other magmatic grains (Fig. 8). Ascribing anomalous sequences or intervals within a core to a specific event is difficult because various mass movement events can produce a sequence similar to the one seen in the core. For example, an earthquake (causing a turbidity current or tsunami) or a flash flood could all be reasonable explanations for this type of sequence to be observed. However, if this turbidite were caused by a flash flood, a fining upward sequence would more frequently be observed since flash floods vary on an annual to decadal time scale (Katz et al., 2015). Therefore, the turbidite sequence was likely caused by an earthquake.

Earthquakes that occurred in the Gulf during a similar time period have been documented by authors such as Kanari et al., 2015, Migowski et al., 2004., Ben-Menahem, 1991 and Karcz et al., 1997. None of the documented earthquakes are stated to have occured at 810 BC, however, many of the time intervals suggested by these studies include the year 810 BC. Kanari et al. (2015) mentions the occurrence of an earthquake between 715 BC and 1095 BC. Their study found anomalous intervals in multiple cores that correspond to this age range. Migowski et al. (2004) investigates Holocene earthquake patterns in the Dead Sea region using radiocarbon dates and varve counting. Their records show an earthquake occurrence at 759 BC with a magnitude of 7.3 and another at 1050 BC at 7.0, both featuring an interval thickness of 5 cm (Migowski et al., 2004). The above mentioned earthquakes cannot be directly attributed to the one ascribed to the turbidite sequence found in the GoA core. However, if provided with more accurate age constraints, it is plausible that these earthquakes may have an imprint on the GoA core.

The most extreme values found in the proxy records occur between 96-87 cm (~810 BC). This interval is highlighted by a grey box, but will be ignored in the text in the 2 subsequent section as it is assumed that this material is allochthones and is unrelated to the variability seen throughout the rest of the record.

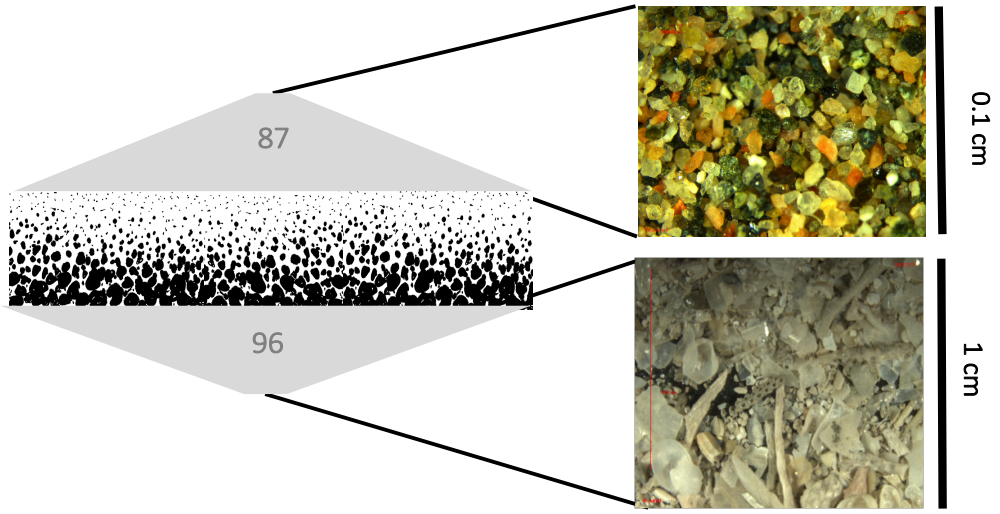

Figure 12 Schematic diagram of turbidite with images of bottom and top sections of the interval.

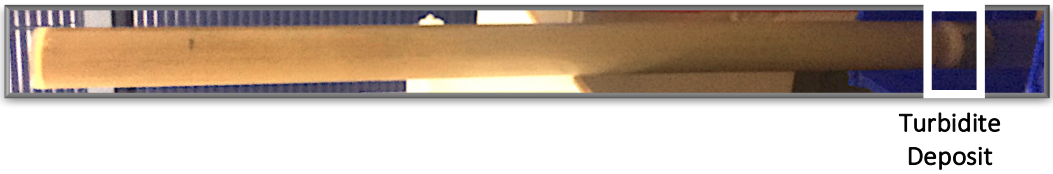

Figure 13 Sediment gravity core with carbonate rich layer attributed to a turbidite deposit (Torfstein, 2016).

Chapter 4: Results

The following sections outline the results of the individual proxy records: Carbonate (%), foraminiferal abundances and geochemistry signatures related to sediment provenance. Measurements were obtained for each cm of the core, but are plotted on a time axis, determined by the age model determined in chapter 3.

4.1 Carbonate (%)

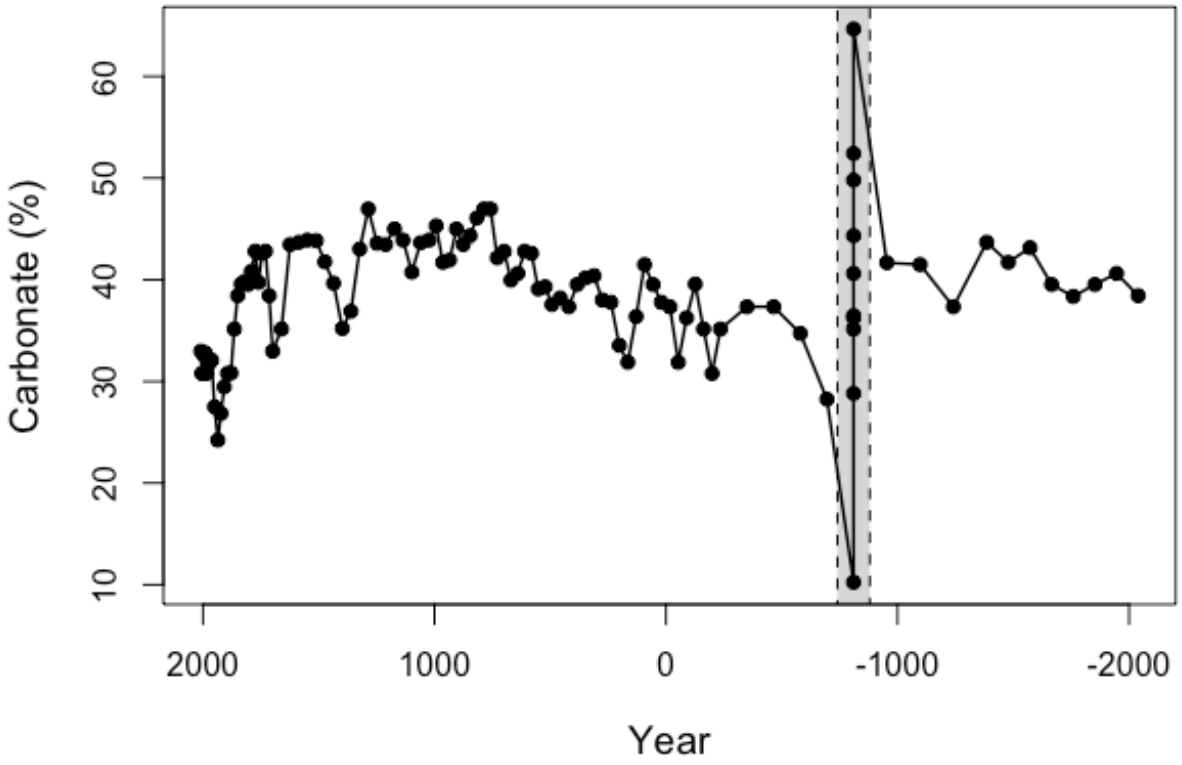

Figure 14 Carbonate (%) measured on 1.00 g of dried sediment, determined by pressure gage.

Carbonate (%) record ranges between 24 ± 1.5% and 47 ± 1.5%. Between 1240 BC and 1950 BC (99-107 cm) carbonate (%) ranges between 37 ± 1.5% and 45 ± 1.5% (Fig. 14). Between 460 BC and 311 AD (84-67 cm) carbonate features 3 periodic oscillations with a 10% change (minimum at 31% and maximum at 40%). Carbonate remains relatively constant between 350 AD and 1286 AD (67-37 cm) at 47 ± 1.5% and 37 ± 1.5%. Between 1286 AD and 1730 AD (37 -24 cm), carbonate % features two troughs, with 10 ± 1.5% variation. At ~1700 AD (24 cm), carbonate (%) begins to decrease from 43 ± 1.5% to 38 ± 1.5%. At approximately 1850, (16 cm), carbonate % begins to decrease at a higher rate, from 38 ± 1.5% to 24 ± 1.5% in ~1936 (10 cm).

The top 8 cm of the core ~ 1963-2016 features constant carbonate (%) at approximately 32%, with minor variations within the error range. The overall trend featured a convex pattern beginning at ~ 500 BC (84 cm) and terminating at the top of the core with the inflection point occurring somewhere between 750 AD – 1250 AD (53 -37 cm).

4.2 Foraminifera picking and identification

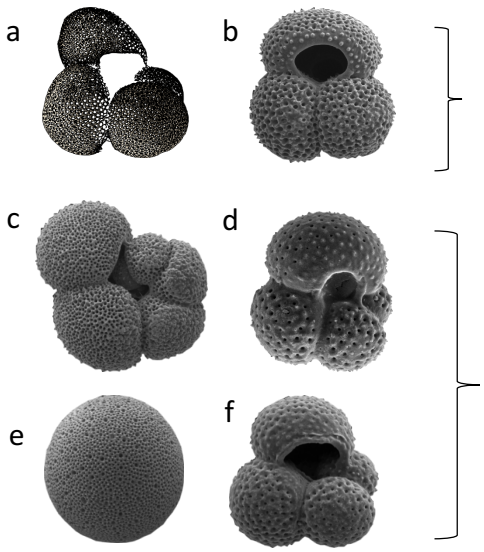

Figure 15 Common Planktonic Foraminifera in the Gulf (SEM photos, courtesy of N. Chernihovsky, 2017)

a) Globerigerinoides sacculifer
b) Globerigerinoides ruber
c) Globigerinella siphoniphera
d) Globoturborotalita tenella
e) Orbulina universa

Total planktonic foraminifera (~10 species) (Fig. 15) ranges from approximately 3 to 55 individuals/g wet sediment (g_{ws}). From the 2000 BC-1500 BC (bottom 5 cm) of the core show an increase from 11 to 44 individuals, followed by a decrease to 20 individuals. Foraminifera values remain low (approximately 4-7 individuals/g_{ws}) from 810 BC to 522 AD (89 to 61 cm) excluding a brief interval between 200 BC and 20 BC (81 and 75 cm) featuring a local maximum of 18 individuals/g_{ws} (Fig. 16 a). This increase is driven by *G. ruber* (Fig. 16 b). Layers above 520 AD (61 cm) feature a steady increase until 820 AD (51 cm), when population increases from 10-40 individuals/g_{ws}. A local maximum at 1200 AD (39 cm) containing 52 individuals is followed by a sharp decrease to 8 individuals/g_{ws} showing a local minima at 1360 AD (35 cm). Population begins to increase again from 1400 AD (34 cm) to 1820 AD (18 cm) featuring 52 individuals.

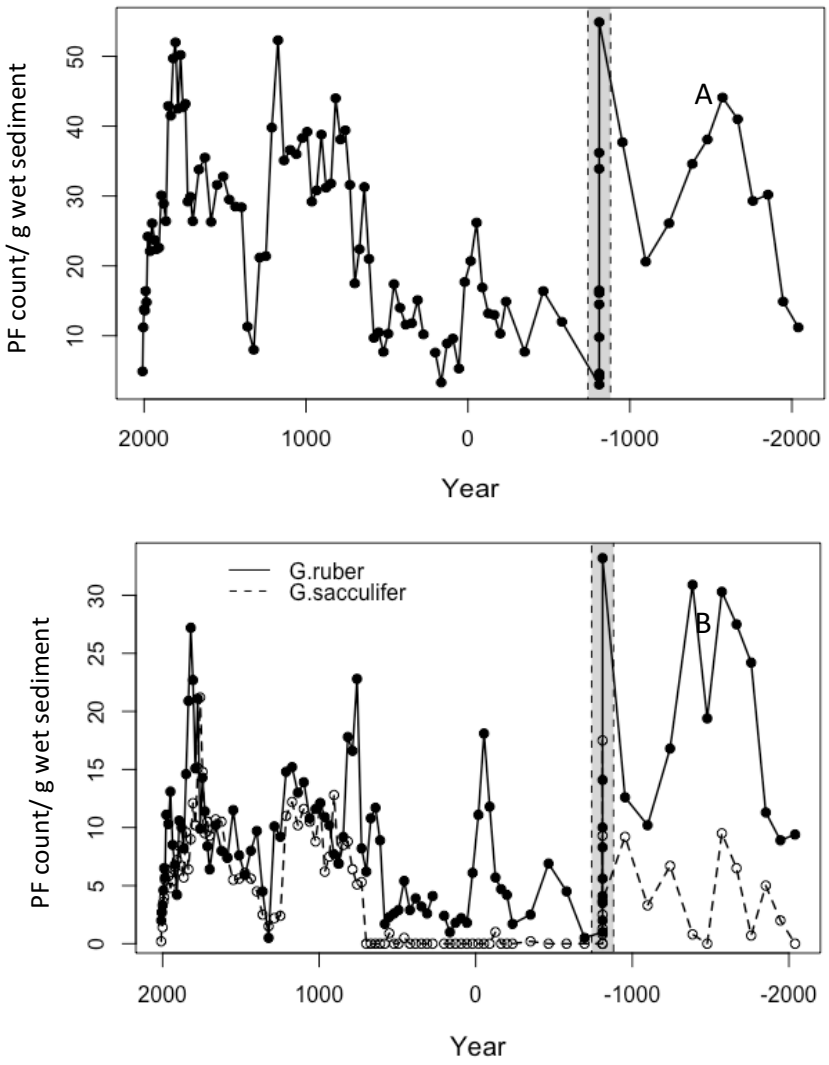

Figure 16 A) Total PF counts, (approximately 8 species) B) G. ruber and G. sacculifer (Dominant PF species in the Gulf).

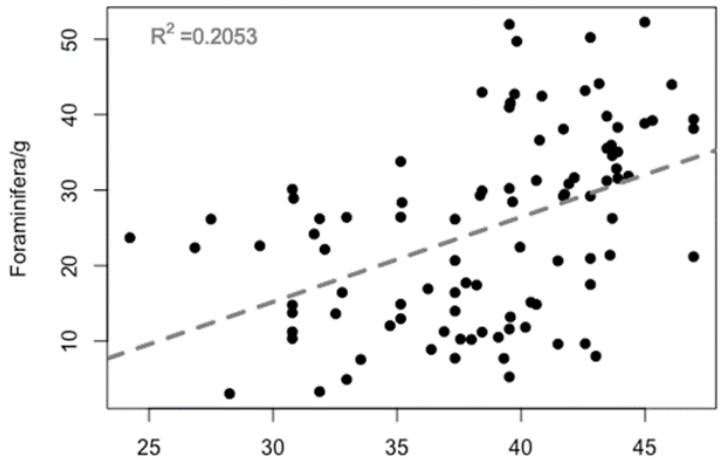

Figure 17 Relationship between carbonate (%) and Foraminifera count, R^2 value of 0.2

Two troughs at 1714 AD (25 cm) and 1880 AD (14 cm) features a decrease to 26 individuals. Foraminifera counts decrease after 1820. *G. sacculifer*, however, have lower abundances than *G. ruber* and are absent between 810 BC and 700 AD (55-90 cm). Throughout the record, *G. ruber* exhibits 3 short intervals of high abundances. Although *G. sacculifer* typically show similar trends to *G. ruber* populations, these *G. ruber* peaks are not reflected in *G. sacculifer* abundances. Between 2000 BC and 810 BC (104-96 cm) *G. ruber* abundances are consistently 2-10 times more abundant than *G. sacculifer*. Between 50 BC and 50 AD (77-74 cm) G. sacculifer abundances remain at 0, *G. ruber,* however, shows an average of 15 individuals/g_{ws}. The last interval that features the largest deviation is between 780-850 AD (52-50 cm) where *G. ruber* (approximately 20 individuals/g_{ws}) is 2-4 times higher than *G. sacculifer* (approximately 5 individuals/g_{ws}). Foraminiferal abundances show low correlation with carbonate (%) record (Fig. 17).

4.3 Sediment provenance: Fe/Al

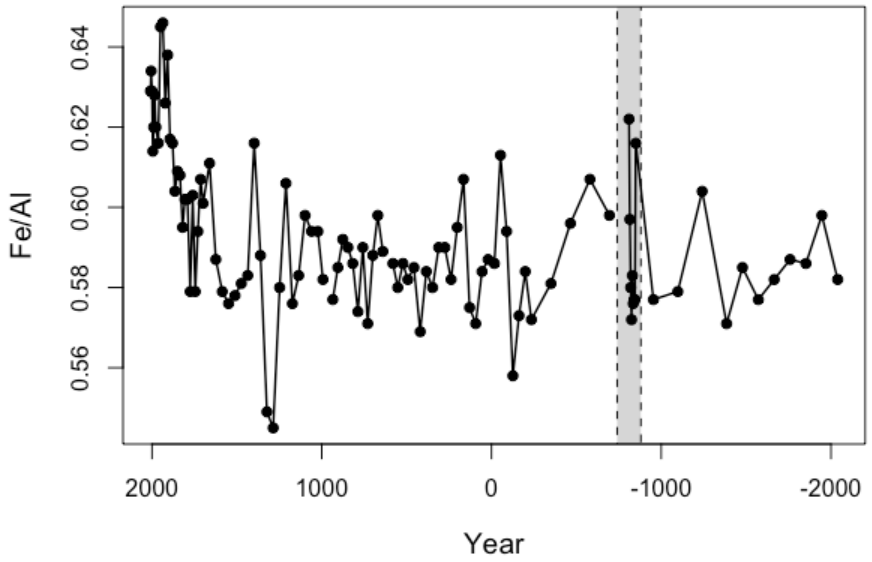

Figure 18 Fe/Al measured on each cm interval measured from the bulk component of geochemistry analysis.

Bulk sediment ratio typically ranges between 0.55 and 0.64. Between 1950 BC and 1791 AD Fe/Al ratios are generally below 0.6. Between 1800 and 2016, (0-20 cm), Fe/Al ratios steadily increase in Fe to a local maximum of 0.65 at 10 cm. At 9 cm (~1960-2016), values begin

to decrease, yet still show higher ratios Fe/Al (0.64 and 0.61) compared to the rest of the core. A down core record minimum of 0.545 occurs at approximately 1323 (37 cm) (Fig. 18).

Chapter 5: Discussion

This chapter will interpret changes in the carbonate, foraminifera, and geochemical proxies and discuss these proxies in context of coeval trends.

5.1 Carbonate Fluctuations

Throughout the core, the carbonate record changes by a factor of 2 (25-50%). Below, are 3 possible mechanisms that could cause such large variations.

5.1.1 Mechanism (1): Dissolution

Dissolution is likely not responsible for the variation in the carbonate record, due to the presence of aragonitic pteropoda (Fig. 19 a and b). Aragonite is a less stable form of $CaCO_3$. An abundance of pteropods were observed in the core, throughout foraminifera picking. A high degree of calcite saturation, between Ω 5-6 suggests that calcite dissolution is highly unlikely in these conditions (Reiss and Hottinger, 1986; Yusuf, 2007; Sultan, 2014).

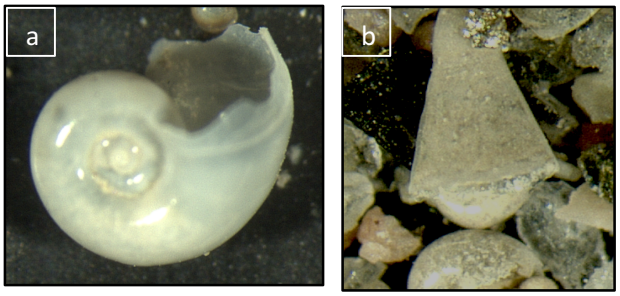

Figure 19 a) Limacina inflata b) Clio Convexa common pteropoda species found in sediment core.

5.1.2 Mechanism (2): Production

In the Gulf of Aqaba, the main carbonate producers are foraminifera, coccolithophora and coral (Reiss and Hottinger, 1984). Between 500-1200 AD and 1300-1700 AD Carbonate (%) and foraminifera abundances both show increases. Throughout the core, however, minor correlations between foraminiferal abundances and carbonate (%) suggests that Foraminifera do not account for the majority of the carbonate material. Other calcareous material, such as pteropoda, coccolithophora, reef fragments and detrital dolomite or limestone from the hinterland likely account for the rest of the carbonate content. Reef fragments and pteropoda were observed in the core, but were not quantified. It is also important to note that during the wet sieving process, only the <125 µm fraction size of sediments were preserved. It was

observed that the majority of the sediments (approximated to be > 50%) accounted for very fine sand, silt and clay sized grains foraminifera and coccolithophora would be included in this fraction and therefore measured during the carbonate (%) measurements, but not during the foraminifera picking process. Thus, production cannot be completely excluded as a mechanism for carbonate fluctuation.

5.1.3 Mechanism (3): Dilution

Dilution is the most likely process that could account for carbonate (%) fluctuation. The Fe/Al geochemical ratio measured on bulk sediments represents non-carbonate material. Since neither of these elements are found in the carbonate component of the sediments, fluctuations in the Fe/Al component likely reflect changes in the source of sediment being delivered to the Gulf. A change in source material would likely also affect the amount of material being delivered into the Gulf. The coincidental fluctuations in the carbonate record may suggest that dilution is a common mechanism (Emery, 1964; Friedman, 1968).

5.2 Sediment provenance

Deposition of granite derived sediment via aeolian and fluvial processes dominate the Gulf (Allison and Niemi, 2010). Comparable Fe/Al ratios of Saharan Dust and the ANS, suggests that granitic sourced sediments maybe transported into the Gulf via Wadi Yutim, Wadi Mubarak, Wadi Arava and others. Fe/Al ratios in the GoA core lie between 0.55 and 0.64 which are similar to Saharan dust, but likely contain material sourced from the continental crust, likely the ANS. The Gulf's sediment Fe/Al ratio are slightly lower than Saharan dust at 0.63±0.02 (Guieu et al., 2002) and higher than upper continental crust ratios of the southeastern Arabian Sea at 0.44 (Pattan et al., 2012). Saharan dust is the world's largest source of aeolian soil dust and likely accounts for almost half of the aeolian material supplied to the world's oceans (Taani et al., 2014). One of the main trajectory pathways of Saharan dust is over the eastern Mediterranean to the Middle East (Goudie and Middleton, 2001).

5.3 Habitat Variability for Planktonic Foraminifera

Foraminifera are single-celled organisms that inhabit marine and freshwater ecosystems (Reiss and Hottinger, 1984). They are excellent paleoenvironmental indicators due to their abundance, diversity, small size, and high capacity for preservation (Reiss et al., 1980; Almogi-Labin, 1982; Arz et al., 2006, Edelman-Furstenberg et al. 2009). They are highly sensitive to

environmental changes and provide excellent proxies for past sea surface temperatures and salinities. Changes in salinity and pycnocline depth, and food availability all affect foraminifera population. Between 800 BC and 700 AD *G. sacculifer* disappears. The occasional presence of PF, within barren intervals, could suggest that salinity may not have been much above or below the tolerable range for *G sacculifer*. Fluctuations in foraminiferal abundances may be related to similar mechanisms that affect the carbonate record. Fluctuations in the foraminifera record may be a result of dissolution, production and/or dilution. Similar to the carbonate record, dissolution is not the cause of foraminifera fluctuations due to the supersaturation of seawater with respect to calcite indicated by Ω 5-6 value and the presence of aragonitic pteropod shells (Reiss & Hottinger, 1984). In the case of foraminifera production, the carbonate record would likely show coeval increases and decreases, however, as mentioned above, foraminifera abundance and carbonate (%) only have minor co-variations. Dilution due to increase in freshwater input bringing in terrestrial material may also influence foraminifera abundances. However, unlike the carbonate record, dilution cannot be ruled out as the primary mechanism because there are no coeval changes in the Fe/Al record. This suggests that there is likely another mechanism that was not accounted for in the data set presented that is affecting foraminiferal abundances.

G. ruber and *G. sacculifer* are typically the two most common species in the Gulf: both dwell in the upper 50 m of the water column, however*, G. sacculifer* typically migrates to greater depths (up to 150 m) and reproduces at approximately 80 m depth or deeper (Bijma and Hemleben, 1994; Reiss et al., 1980, 1999; Reiss and Hottinger, 1984). *G. ruber* are herbivorous and prey on plankton, and thrive in 25 °C surface waters while *G. sacculifer* are carnivorous and consume mostly calanoid copepods and partly on algae (Auras-Schudnag et al., 1989; D'Orbigny, 1839; Thirumalai et al., 2014; Anderson, 1983). It is difficult to discern or associate specific hydrological patterns that cause PF barren zones, or fluctuations in the record because there are a variety of complex mechanisms that have potential to cause fluctuations that work together and independently.

In the 1980's *G. sacculifer* populations began to decline and completely disappear in 1990. This time interval is not analyzed at a high enough resolution in the GoA core to determine if these ages correspond directly, however, a decline in both *G. ruber* and *G.*

sacculifer is observed in the top 7 cm which dates to approximately 1977. This interval coincides with a period of increased nutrient loading from anthropogenic sources (Oron et al., 2014), likely causing an unsuitable environment for *G. saccullifer* and likely the organisms they feed on. Diet plays an essential role in foraminifera abundances. In general, low nutrient levels may partly explain a decrease in *G. ruber*, while food quality and variety may account for *G. sacculifer* abundances. Diet, however, would likely show a coeval maxima and minima between *G. sacculifer* and *G. ruber* abundances since copepods consume phytoplankton which are dependent on nutrients, much like *G. ruber*. The coeval increases and decreases are featured in the GoA core.

5.4 Summary of interpretations and application to climate

Changes in sedimentation rates are likely related to changes in the amount of terrestrial material transported to the Gulf. Flash floods transporting large quantities of sediments (Fig. 20 a and b) and Saharan dust are likely responsible for the majority of the terrestrial input into the Gulf.

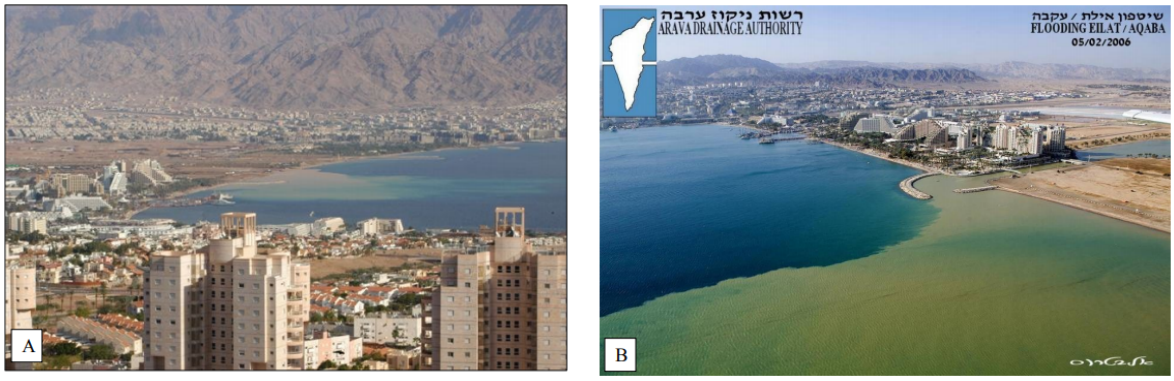

Figure 20 Flooding event in 2010 in the Gulf of Aqaba (Goodman Lecture, 2010)

However, the effects of sediment mobilization and supply are difficult to correlate to specific processes. Changes in the amount of sediment delivered via dust storms or flash floods are likely influenced by changes in precipitation which may be related to variations in humidity intensity which typically last between 1200-1500 years (Legge et al., 2006; Arz et al.,2003, Lamy et al., 2006, Edelman-Furstenberg et al., 2009). The driving forces of the late Holocene climatic changes are widely debated. Arz et al. (2003) claim that humid climates are caused by fluctuations in the Mediterranean climate, since monsoonal rains do not extend far enough northwards. Other sources, such as Moustafa et al. (2000), suggest that humid conditions are

caused by the northward migration of African monsoons, correlated to a decrease in coral reef growth rates.

Changes in sediment input are also associated with water diversion engineering, water drainage management systems and agricultural terraces built during the past 4000 years, may also have a small influence on sedimentation processes (Khalil and Schmidt, 2009). The Chalcolithic, Iron Hellenistic, Roman, Islamic, Mamluk and Ottomon empires all inhabited the Gulf region for various time periods during the last ~4000 years (Allison and Niemi, 2010). Infrastructure that was destroyed by earthquakes and re-built may have minor effects on the amount and location of sediment delivery.

Down-core proxy records, when compared to one another, show coeval changes in the recent 500 years. This trend corresponds to the dilution effect, likely caused by an increase in dust storms and flash floods. Other anomalous intervals, however, generally do not coincide with other proxy records, for example, low foraminifera abundances between ~ 800 BC until ~ 700 AD and therefore cannot be mechanistically linked to any specific climatic or hydrographic variation (Fig. 21).

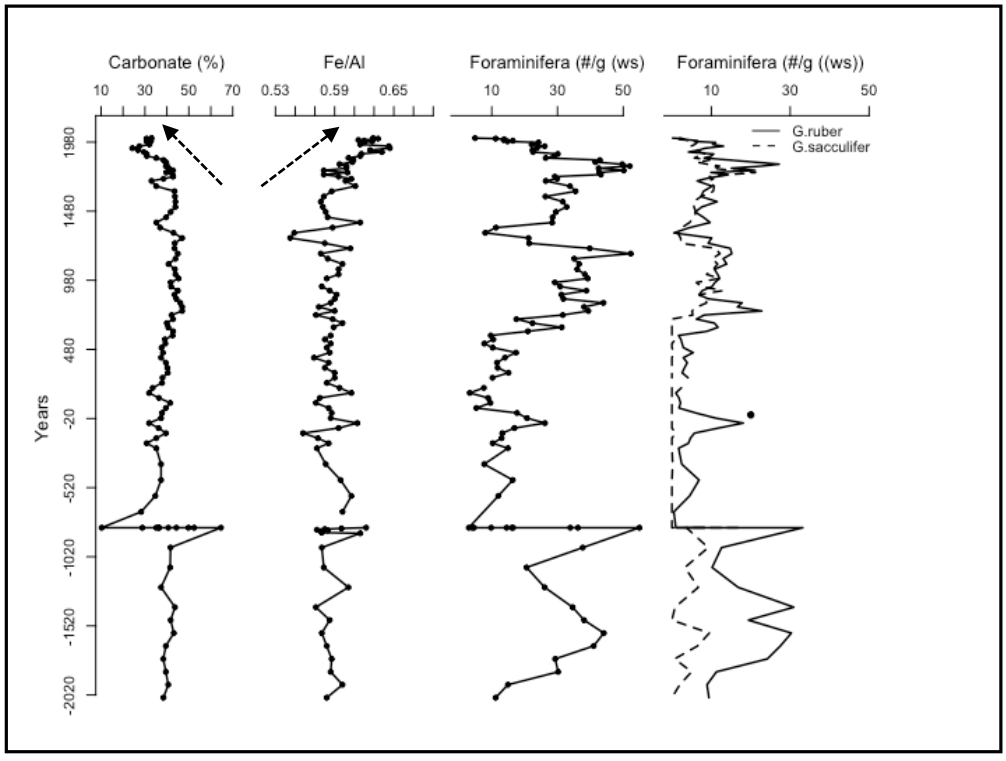

Figure 21 Down-core record comparing proxies and intervals of interest.

6.0 Conclusion

The 107 cm gravity core from the Gulf of Aqaba recovered from 720 m water depth is partially composed of carbonate sediments, rich in foraminifera, pteropoda and reef fragments. The core also contains a significant amount of terrestrial material transported during high flux events that occur on short time scales, likely on the order of days. This includes mineral dust transported by wind from the Saharan desert as well as granitic sourced sediment delivered by flash floods through Wadis. These processes dilute the carbonate component and are therefore likely responsible for the large fluctuations seen in the carbonate record. Production of carbonate may also contribute to carbonate fluctuations but likely to a much lesser extent. Dissolution does not occur in the Gulf and therefore does not affect the carbonate record.

The Gulf is also susceptible to mass movement events caused by earthquakes due to it's proximity to the Dead Sea Transform fault. An interval between 87-96 cm is tentatively ascribed to a turbidite triggered by an earthquake. Finally, with the aid of accurate age assignments, changes in proxy records and sedimentation rates are used to reconstruct past climate and paleoenvironmental settings.

References

Allision, A and Niemi, T. 2010. Paleoenvironmental Reconstruction of Holocene Coastal Sediments Adjacent to Archaeological Ruins in Aqaba, Jordan. Geoarchaeology, **52:** 5.

Almogi-Labin, A., Hemleben, C., Meischner, D., Erlenkeuser, H. 1996. Response of Red Sea deep-water agglutinated foraminifera to water mass changed during the Late Quaternary. Marine Micropaleotology **28:** 283-297.

Al-Rousan, S., Rasheed, M., Al-Horani, F., and Manasrah, R. 2006. Geochemical and Textural Properties of Carbonate and Terrigenous Sediments along the Jordanian Coast of the Gulf of Aqaba. Journal of Oceanogrpahy, **63:** 839-849.

Anderson, O.R. 1983. Radiolaria. Springer, New York, pp: 352.

Arz, H., Lamy, F., Patzold, J., Muller, P., Prins, M. 2003. Mediterranean Moisture Source for an Early Holocene Humid Period in the Northern Red Sea. Science, **300** (5616): 118-121.

Auras-Schudnagies, A., Kroon., Ganssen, G., Hemleben, C., Van Hinte, J. 1989. Distributional pattern of planktonic foraminifers and pteropods in surface waters and top core sediments of the Red Sea, Gulf of Aden and western Arabian Sea, controlled by the monsoonal regime and other ecological factors. Deep-Sea Res., **36:** 1515-1533.

Ben-Menahem, A. 1991. Four Thousand Years of Seismicity along the Dead Sea Rift. J. Geophys. Res, **96:** 20195-20216.

D'orbigny. 1839. Globerigeinoides ruber [online]: Available from https://www.ngdc.noaa.gov/mgg/geology/hh1996/ruber.html

Edelman-Furstenberg, Y., Almogi-Labin, A., Hemleben, C. 2009. Palaeoceanogrpahic evolution of the central Red Sea during the late Holocene. The Holocene **19**,1: 117-127.

Edelman-Furstenberg, Y., Scherbacher, M., Hemleben, C., Almogi-Labin, A. 2001. Deep-Sea Benthic Foraminifera form the central Red Sea. Journal of Foraminiferal Research **31**: 48-59.

Fenton, M., Geiselhart, S., Rohling, E., Hemleben, Ch. 2000. Aplanktonic zones in the Red Sea. Marine Micropaleontology; **40:** 277-294.

Friedman, G. 1968. Geology and Geochmistry of Reefs, Carbonate Sediemnts, and Water, Gulf of Aqaba (Elat), Red Sea.Journal od Sedimentary Research **38:** 895-919. (only abstract)

Goodman-Tchernov, B., Katz, T., Shaked, Y., Qupty, N., Kanari, M., Niemi, T. et al., 2016. Offshore Evidence of an Undocumented Tsunami Event in the 'Low Risk' Gulf of Aqaba-Eilat Northern Red Sea. PLoS ONE 11(1).

Goudie, A. and Middleton, N. 2001. Saharan dust storms: nature and consequences. Earth-Science Reviews, **56:** 179-204.

Hottinger, L., Reiss, Z. 1984. The Gulf of Aqaba: Ecological Micropaleontology. Springer-Verlag Berlin Heideberg New York Tokyo, Germany.

Kanari, M., Ben Avraham, Z., Tibor, G., Bookman, R., et al, 2015. On-land & Offshore Evidence for Holocene Earthquakes in the Northern Gulf of Aqaba-Elat, Israel/Jordan. INQUA Focus Group on Paleoseismology and Active Tectonics.

Karcz, I., Kafri, U., Meshel, Z. 1977. Archeological evidence for subrecent seismic activity along the Dead Sea-Jordan rift. Nature **269:** 234-235.

Katz O. Beyth M. Miller N. Stern R. Avigad D. Basu A. Anbar A. 2004, A Late Neoproterozoic (∼630Ma) Boninitic Suite from southern Israel: Implications for the Consolidation of Gondwanaland: Earth and Planetary Science Letters **218:** 475-490, doi: 10.1016/S0012-821X(03)00635-6.

Katz, T., Ginat, H., Eyal, G., Steiner, Z., Braun, Y., Shalev, S., Goodman-Tchernov, B. 2015. Desert flash floods from hyperpycnal flows in the coral-rich Gulf of Aqaba, Red Sea. Earth and Planetary Science Letters. Vol 417, 87-98.

Khalil, L and Schmidt, K. 2009. Prehitoric 'Aqaba I. Orient-Archaologie Band 23. Rahden/Westfalen, Germany: Verlag Marie Leidorf.

Kumar, K., Band, S., Ramesh, R., Awasthi, N. 2018. Monsoon variability and upper ocean stratification during the last ~ 66 ka over the Andaman Sea: inference from the d18O records of planktonic foraminifera. Quaternary International. IN PRESS.

Lamy, F., Arz, H., Bond, C., Bahr., Patzold, J. 2006. Multicentennial-sclae hydrological changes in the Black Sea and northern Red Sea during the Holocene and Arctic/North Atlantic Oscillation. Paleoceanography **21**, PA 1008.

Migowski, C., Agnon, A., Bookman, R., Negendank, J., Stein, M. 2004. Recurrence pattern of Holocene earthquakes along the Dead Sea transform revealed by varve counting and radiocarbon dating of lacustrine sediments. Earth and Planetary Science Letters **222**: 301-314.

Oeschger H, Siegenthaler U, Schotterer U, Gugelmann A. 1975. A box diffusion model to study the carbon dioxide exchange in nature. Tellus 27(2):168–92.

Palchan, D., Stein, M, Almogi-Lacin, A, Erel, Y. and Goldstein, S. 2013. Dust transport abd synoptic conditions over the Sahara-Arabia deserts during the MIS6/5 and 2/1 transitions from grain-size, chemical and isotopic properties of Red Sea cores. Earth and Planetary Science Letters **382:** 125-139.

Reimer, P., Bard, E., Bayliss, A., Beck, J., Blackwell, P., Bronk Ramsey, C., et al., 2013. IntCal13 and Marine13 radiocarbon age calibration curves 0–50,000 years cal BP. Radiocarbon **55**(4):1869–1887.
Reimer, P.J., Baillie, M.G.L., Bard, E., Bayliss, A., Beck, J.W., Bertrand, C.J.H., Blackwell, P.G., Buck, C.E., Burr, G.S., Cutler, K.B., Damon, P.E., Edwards, R.L., Fairbanks, R.G., Friedrich, M., Guilderson, T.P., Hogg, A.G., Hughen, K.A., Kromer, B., McCormac, G., Manning, S., Ramsey, C.B., Reimer, R.W., Remmele, S., Southon, J.R., Stuiver, M., Talamo, S., Taylor, F.W., van, d.P.J., Weyhenmeyer, C.E., 2004. IntCal04 terrestrial radiocarbon age calibration, 0–26 cal kyr BP. Radiocarbon **46,** 1029–1058.

Riehl and Kienast, 2017. High Resolution Sediment Trap, Gulf of Aqaba [Preliminary Research].

Shaked, Y., Agnon, A., Lazar, B., Marco, S., Avner, U. and Stein, M. 2004. Large earthquakes kill coral reefs at the north-west Gulf of Aqaba. Terra Nova **16:** 133-138.

Shaked, Y., Marco, S., Lazar, B., Steiner, M., Cohen, C., Sass, E., Agnon, A. 2001. Late Holocene shorelines at the Gulf of Aqaba: migrating shorelines under conditions of tectonic and sea level stability. Stephen Mueller Special Publication Series 2: 105-111.

Stein, M, Almogi-Labin, A., Goldstine, S., Hemleben, C., Starinsky, A. 2007. Late Quaternary changes in desert dust inputs to the Red Sea and Gulf of Aden from 87Sr/86Sr ratios in deep-sea core. Earth and Planetary Science Letters **261:** 104-119.

Steiner, Z., Lazar, B., Levi, S. et al, 2016. The effect of bioturbation in pelagic sediments: Lessons from radioactive tracers and planktonic foraminifera in the Gulf of Aqaba, Red Sea. Geochemia et Cosmochimica Acta **194**: 139-152.

Steiner, Z., Lazar, B., Torfstien, A., Erez, J. 2017. Testing the utility of geochemical proxies of paleoproductivity in oxic sedimentary marine settings of the Gulf of Aqaba, Red Sea. Chemical Geology **473**, 40-49.

Stuiver, M., Paula, R., Braziunas, T. 1998. High Precision Radiocarbon Age Calibration for Terrestrial and Marine Samples. Radiocarbon; **40**: 1127-1151.

Thirumalai, K., Richey, J., Quinn, T., Poore, R. 2014. Globergerinoides ruber morphotypes in the Gulf of Mexico: A test of null hypothesis. Scientific Reports **4:** 6018.

Tibor, G., Niemi, T.M., Ben-Avraham, Z., et al, 2010. Active Tectonic morphology and submarine deformation of the norther Gulf of Eilat/Aqaba from analyses of multibeam data. Geo-Mar Lett **30**, 561-573.

Trommer, G., Siccha, M., Rohling, E., Grant, K., T.J. van der Meer, M., Schouten, S., Hemleben, C., and Kucera, M. 2010. Millenial-scale variability in Red Circulation in Response to Holocene Insolation Forcing. Paleoceanography; **25:** PA3203, doi:10.1029/2009PA001826.

Wurgaft, E., Shamir, O., Barkan, E., Paldor, N., and Luz, B. 2013. Mixing processes in the deep water of the Gulf of Elat (Aqaba): Evidence from measurements and modeling of the triple isotopic composition of dissolved oxygen. Limnological Oceanography. **4:** 1373-1386.

Yusuf, N. 2007. Paleoenvironmental Conditions as Recorded by Globigerinoides Sacculifer and Globigerinoides Ruber from the Northern Red Sea. Journal of Applied Sciences **7:** 155-164.

Appendix A

Raw values for proxy data

Core Depth (cm)	*Year*	*carbonate (%)*	*total foram (#/g wet sed.)*	*G. ruber (#/g wet sed.)*	*G. sacculifer (#/g wet sed.)*	*Fe/Al*
1	2016	32.97	4.9	2.0	0.2	0.629
2	2009	30.78	11.2	2.7	2.7	0.634
3	2005	30.78	13.8	3.3	1.4	0.629
4	2000	32.53	13.6	4.6	3.6	0.614
5	1995	32.79	16.4	6.5	4.0	0.620
6	1990	30.78	14.8	5.7	5.5	0.628
7	1985	31.66	24.2	11.1	6.4	0.620
8	1977	32.09	22.1	10.3	5.8	0.616
9	1963	27.5	26.1	13.1	4.8	0.645
10	1950	24.23	23.7	8.5	5.4	0.646
11	1936	26.85	22.4	6.8	6.6	0.626
12	1922	29.47	22.6	4.2	7.2	0.638
13	1908	30.78	30.1	10.6	8.4	0.617
14	1894	30.83	28.9	10.0	6.7	0.616
15	1879	35.15	26.4	8.2	5.7	0.604
16	1865	38.43	42.9	14.6	9.6	0.609
17	1850	39.57	41.5	20.9	6.4	0.608
18	1835	39.83	49.7	27.2	9.0	0.595
19	1820	39.53	52.0	22.7	12.1	0.602
20	1806	40.84	42.5	15.1	10.2	0.602
21	1791	42.8	50.2	21.1	15.1	0.579
22	1775	39.74	42.7	9.9	21.2	0.603
23	1760	42.59	43.2	14.3	14.8	0.579
24	1745	42.8	29.2	11.4	9.5	0.594
25	1730	38.43	29.9	8.4	10.5	0.607
26	1714	32.97	26.4	6.4	9.3	0.601
27	1699	35.15	33.8	10.2	10.7	0.611
28	1661	43.46	35.5	8.0	10.5	0.587
29	1624	43.68	26.3	7.4	7.4	0.579
30	1586	43.9	31.6	11.5	5.5	0.576
31	1549	43.85	32.8	7.6	5.6	0.578
32	1511	41.76	29.5	5.9	6.1	0.581
33	1474	39.66	28.5	8.0	5.6	0.583
34	1436	35.2	28.4	9.7	4.5	0.616

35	1398	36.9	11.3	4.5	2.5	0.588
36	1361	43.02	8.0	0.5	1.5	0.549
37	1323	46.96	21.2	10.1	2.2	0.545
38	1286	43.59	21.4	9.2	2.4	0.580
39	1248	43.46	39.8	14.8	11.0	0.606
40	1211	44.99	52.3	15.2	12.2	0.576
41	1173	43.9	35.1	13.0	10.2	0.583
42	1136	40.75	36.6	13.9	11.6	0.598
43	1098	43.64	36.0	10.8	10.5	0.594
44	1060	43.9	38.3	11.6	8.8	0.594
45	1023	45.3	39.2	12.1	12.1	0.582
46	993	41.71	29.2	10.9	6.2	NA
47	964	41.93	30.8	10.2	7.5	0.577
48	935	44.99	38.8	7.7	12.8	0.585
49	905	43.46	31.2	6.9	6.9	0.592
50	876	44.33	31.8	9.2	8.5	0.590
51	846	46.08	44.0	17.8	8.8	0.586
52	817	46.96	38.1	16.6	6.4	0.574
53	787	46.96	39.4	22.8	5.1	0.590
54	758	42.15	31.6	8.2	5.3	0.571
55	729	42.8	17.5	6.2	0.0	0.588
56	699	39.96	22.4	10.8	0.0	0.598
57	670	40.62	31.3	11.7	0.0	0.589
58	640	42.8	21.0	8.9	0.0	NA
59	611	42.59	9.7	1.7	0.0	0.586
60	581	39.09	10.5	2.3	0.9	0.580
61	552	39.31	7.7	2.6	0.0	0.586
62	522	37.56	10.3	2.9	0.0	0.582
63	493	38.21	17.4	5.4	0.5	0.585
64	457	37.34	14.0	2.9	0.0	0.569
65	420	39.53	11.6	3.9	0.0	0.584
66	384	40.18	11.8	3.2	0.0	0.580
67	347	40.4	15.1	2.6	0.0	0.590
68	311	38	10.2	4.1	0.0	0.590
69	275	37.78	NA	NA NA		0.582
70	238	33.54	7.6	2.4	0.0	0.595
71	202	31.88	3.3	1.0	0.0	0.607
72	165	36.38	8.9	1.8	0.0	0.575
73	129	41.49	9.6	2.2	0.0	0.571
74	93	39.53	5.3	1.8	0.0	0.584

75	56	37.78	17.7	6.1	0.0	0.587
76	20	37.34	20.7	11.1	0.0	0.586
77	-17	31.88	26.2	18.1	0.0	0.613
78	-53	36.25	16.9	11.8	0.0	0.594
79	-89	39.57	13.2	5.7	1.0	0.558
80	-126	35.15	13.0	4.7	0.0	0.573
81	-162	30.78	10.3	4.2	0.0	0.584
82	-199	35.15	14.9	1.7	0.0	0.572
83	-235	37.34	7.7	2.5	0.2	0.581
84	-350	37.34	16.4	6.9	0.0	0.596
85	-465	34.72	12.0	4.5	0.0	0.607
86	-580	28.25	3.0	0.5	0.0	0.598
87	-810	10.24	4.6	1.0	0.0	0.991
88	-810	28.82	9.8	4.1	0.0	0.622
89	-810	36.25	4.1	2.0	0.0	0.597
90	-810	35.15	14.5	8.3	0.8	0.580
91	-810	36.47	NA	NA	NA	0.572
92	-810	40.62	16.5	3.5	1.3	0.583
93	-810	44.33	16.1	5.6	2.5	0.576
94	-810	49.8	33.9	14.1	9.3	0.577
95	-810	52.42	36.2	10.0	17.5	0.577
96	-810	64.66	54.9	33.2	3.7	0.616
97	-953.75	41.67	37.7	12.6	9.2	0.577
98	-953.75	41.49	20.6	10.2	3.3	0.579
99	-1097.5	37.34	26.1	16.8	6.7	0.604
100	-1241.25	43.68	34.6	30.9	0.8	0.571
101	-1385	41.71	38.1	19.4	0.0	0.585
102	-1478.5	43.15	44.1	30.3	9.5	0.577
103	-1572	39.53	41.0	27.5	6.5	0.582
104	-1665.5	38.35	29.3	24.2	0.7	0.587
105	-1759	39.53	30.2	11.3	5.0	0.586
106	-1852.5	40.62	14.9	8.9	2.0	0.598
107	-1946	38.43	11.2	9.4	0.0	0.582

Appendix B

Pressure gage readings and calibrations for Calcium Carbonate Measurements

Sample Weight= 1.00 g (scale fluctuate b/w 1.00g and 1.01g)

Sample	CaCO3 (PSI)	Final (PSI)	Total Carbonate (%)	CaCO3 (%)	(Mg,Ca)(CO3)2 (%)
	30 seconds	20 (30) minutes	Slope=	Intercept/ Syringe Pressure=	
			189.4	**3.458**	
1	62.05	75.84	38.22	30.94	7.28
2	57.92	72.39	36.40	28.75	7.64
3	58.26	72.39	36.40	28.93	7.46
4	60.33	75.15	37.85	30.03	7.83
5	60.33	75.57	38.07	30.03	8.05
6	56.88	72.39	36.40	28.21	8.19
7	58.61	73.77	37.13	29.12	8.01
8	59.98	74.46	37.49	29.84	7.64
9	52.40	67.22	33.67	25.84	7.83
10	47.92	62.05	30.94	23.47	7.46
11	51.71	66.19	33.12	25.48	7.64
12	55.16	70.33	35.31	27.30	8.01
13	58.61	72.39	36.40	29.12	7.28
14	58.61	72.46	36.43	29.12	7.32
15	64.81	79.29	40.04	32.39	7.64
16	69.29	84.46	42.77	34.76	8.01
17	71.71	86.25	43.71	36.03	7.68
18	72.39	86.67	43.93	36.40	7.54
19	71.57	86.18	43.68	35.96	7.72
20	72.74	88.25	44.77	36.58	8.19
21	76.39	91.36	46.41	38.51	7.90
22	72.26	86.53	43.86	36.32	7.54
23	75.77	91.01	46.23	38.18	8.05
24	75.84	91.36	46.41	38.22	8.19
25	69.29	84.46	42.77	34.76	8.01
26	62.05	75.84	38.22	30.94	7.28
27	65.50	79.29	40.04	32.76	7.28
28	77.4971024	92.39	46.95	39.09	7.86
29	77.91	92.73	47.14	39.31	7.83
30	78.60	93.08	47.32	39.67	7.64
31	77.57	93.01	47.28	39.13	8.15

32	75.70	89.70	45.53	38.14	7.39
33	72.26	86.39	43.79	36.32	7.46
34	65.50	79.36	40.07	32.76	7.32
35	67.22	82.05	41.49	33.67	7.83
36	76.53	91.70	46.59	38.58	8.01
37	82.81	97.91	49.87	41.89	7.97
38	78.60	92.60	47.06	39.67	7.39
39	76.88	92.39	46.95	38.76	8.19
40	79.29	94.80	48.23	40.04	8.19
41	78.60	93.08	47.32	39.67	7.64
42	72.74	88.12	44.70	36.58	8.12
43	76.19	92.67	47.10	38.40	8.70
44	77.57	93.08	47.32	39.13	8.19
45	79.84	95.29	48.48	40.33	8.15
46	73.77	89.63	45.50	37.13	8.37
47	75.36	89.98	45.68	37.96	7.72
48	79.29	94.80	48.23	40.04	8.19
49	75.84	92.39	46.95	38.22	8.74
50	79.22	93.77	47.68	40.00	7.68
51	81.36	96.53	49.14	41.13	8.01
52	82.67	97.91	49.87	41.82	8.05
53	81.70	97.91	49.87	41.31	8.55
54	75.84	90.32	45.86	38.22	7.64
55	75.84	91.36	46.41	38.22	8.19
56	72.88	86.87	44.04	36.65	7.39
57	72.39	87.91	44.59	36.40	8.19
58	75.50	91.36	46.41	38.04	8.37
59	75.15	91.01	46.23	37.85	8.37
60	70.67	85.50	43.31	35.49	7.83
61	68.95	85.84	43.50	34.58	8.92
62	68.81	83.08	42.04	34.50	7.54
63	70.33	84.12	42.59	35.31	7.28
64	68.95	82.74	41.86	34.58	7.28
65	69.29	86.18	43.68	34.76	8.92
66	71.02	87.22	44.22	35.67	8.55
67	71.71	87.56	44.41	36.03	8.37
68	67.22	83.77	42.40	33.67	8.74
69	66.19	83.43	42.22	33.12	9.10
70	60.67	76.74	38.69	30.21	8.48
71	57.92	74.12	37.31	28.75	8.55
72	65.50	81.22	41.06	32.76	8.30

73	71.71	89.29	45.32	36.03	9.28
74	68.26	86.18	43.68	34.21	9.46
75	67.71	83.43	42.22	33.92	8.30
76	67.57	82.74	41.86	33.85	8.01
77	59.29	74.12	37.31	29.48	7.83
78	66.19	81.01	40.95	33.12	7.83
79	70.67	86.25	43.71	35.49	8.23
80	63.78	79.29	40.04	31.85	8.19
81	57.92	72.39	36.40	28.75	7.64
82	62.74	79.29	40.04	31.30	8.74
83	65.50	82.74	41.86	32.76	9.10
84	67.22	82.74	41.86	33.67	8.19
85	62.74	78.60	39.67	31.30	8.37
86	52.40	68.40	34.29	25.84	8.45
87	27.58	39.99	19.29	12.74	6.55
88	53.09	69.29	34.76	26.20	8.55
89	68.95	81.01	40.95	34.58	6.37
90	64.60	79.29	40.04	32.28	7.75
91	65.50	81.36	41.13	32.76	8.37
92	70.46	87.91	44.59	35.38	9.21
93	76.53	93.77	47.68	38.58	9.10
94	84.25	102.39	52.23	42.66	9.57
95	86.87	106.52	54.42	44.04	10.37
96	110.32	125.83	64.61	56.42	8.19
97	72.46	89.56	45.46	36.43	9.03
98	72.39	89.29	45.32	36.40	8.92
99	67.91	82.74	41.86	34.03	7.83
100	76.19	92.73	47.14	38.40	8.74
101	73.08	89.63	45.50	36.76	8.74
102	74.12	91.91	46.70	37.31	9.39
103	69.02	86.18	43.68	34.61	9.06
104	68.95	84.32	42.70	34.58	8.12
105	68.26	86.18	43.68	34.21	9.46
106	72.39	87.91	44.59	36.40	8.19
107	63.78	84.46	42.77	31.85	10.92

Appendix C

Sediment Trap Data: Linear Sedimentation rates for various depths (Riehl, 2017)

AVERAGE 2014	**TOTAL**	**0.089**
	570 m	0.185
	450 m	0.169
	400 m	0.080